Air-stable, non-volatile resistive memory based on hybrid organic/inorganic nanocomposites

CrossMark

Giulia Casula [a],[*], Piero Cosseddu [b], Yan Busby [c], Jean-Jacques Pireaux [c], Marcin Rosowski [d], Beata Tkacz Szczesna [d], Katarzyna Soliwoda [d], Grzegorz Celichowski [d], Jaroslaw Grobelny [d], Jiří Novák [e],[f], Rupak Banerjee [f], Frank Schreiber [f], Annalisa Bonfiglio [a]

[a] University of Cagliari, Dept. of Electrical and Electronic Engineering, Piazza D'Armi, 09123 Cagliari, Italy
[b] CNR – Institute of Nanoscience, S3 Centre, Via Campi 213A, 41100 Modena, Italy
[c] University of Namur, Research Center in Physics of Matter and Radiation (PMR), Laboratoire Interdisciplinaire de Spectroscopie Electronique (LISE), rue de Bruxelles 61, B-5000 Namur, Belgium
[d] University of Lodz, Department of Materials Technology and Chemistry, Pomorska St. 163, 90-236 Lodz, Poland
[e] Central European Institute of Technology, Masaryk University, Kamenice 5, CZ-62500 Brno, Czech Republic
[f] Institute of Applied Physics, Eberhard-Karls-Universität Tübingen, Auf der Morgenstelle 10, D-72076 Tübingen, Germany

ARTICLE INFO

ABSTRACT

A non-volatile memory element based on organic/inorganic nanocomposites is presented. The device can be operated in ambient conditions, showing high retention time and long-term life time. The formation/rupture of metallic filaments in the organic matrix is investigated by HR-XPS and ToF-SIMS analysis, and is demonstrated to be the driving mechanism for the resistive switching.

© 2015 Elsevier B.V. All rights reserved.

1. Introduction

Organic semiconductor devices have been widely studied for different applications, from sensing to optoelectronics [1–4]. Compared to the inorganic semiconductor technology, organic devices exhibit a variety of attractive advantages such as the possibility of low cost fabrication over large areas, of using flexible substrates, and of exploiting printing techniques [5–10].

In order to extend the application of organic semiconductors to more complex electronic systems, memory elements are essential. For these reasons, recently there has been a significant amount of research on memory devices based on organic materials [11–13]. Among them, organic Resistive Random Access Memories (RRAMs) [14] have emerged as promising candidates for future information storage media due to their attractive properties, including simple structure, good retention time, and high endurance. In addition, organic memories can show non-volatile characteristics or, in other words, can retain the stored information even when the electrical power supply has been turned off.

The key function of RRAM devices is the resistive switching: the resistance of the memory can be reversibly switched between two stable resistive states (low and high) by applying appropriate voltage pulses. So far, several materials have been studied for RRAM applications, and many groups have demonstrated the resistive switching in several types of organic and polymeric materials with different device structures [15–17]. Organic resistive

* Corresponding author.
E-mail address: giulia.casula@diee.unica.it (G. Casula).

memories were first introduced by Ma et al. [18] in 2002. They proposed a promising bi-stable device consisting of a three-layer-structure (organic/metal/organic) comprised between two metal electrodes. Initially, the idea was that the metal interlayer should be an ultra-thin continuous floating layer. However, detailed investigations revealed that this metal interlayer is electrically discontinuous, as it actually consists of small isolated metal clusters or nanoparticles (NPs) [19]. The Yang group extended this approach to different systems [20–23] and their research has stimulated strong interest in this field [24–26]. Recently, Liu and co-workers [27] proposed organic non-volatile memories based on $Au/Alq_3/metal$ nanoparticles/ Alq_3/Al. In particular, they concluded that the electrical characteristics of devices with gold NPs display much better performances with respect to those with aluminum NPs. These devices showed reproducible resistive switching, a high on/off current ratio of about 10^4, a retention time of 4 h and a reasonable stability under bias stress test.

Despite these promising performances, organic bi-stable memory devices are still in the exploratory stage of the research. Several important issues, such as the physical explanation of the resistive switching behavior, are still not clear. Although a remarkable amount of research has been made and many plausible mechanisms have been proposed by different groups, the understanding of the resistive switching phenomena is still controversial. Furthermore, their stability and reliability are still debatable. Indeed, organic memories should benchmark against inorganic FLASH memories in terms of data retention time, number of operation cycles, power consumption and stability in ambient conditions, in order to allow them to be employed in commercial products. However, one of the main issues concerning the real employment of such devices in operational environment deals with their long time stability. Indeed, many reported works show excellent behaviors but the devices have been only characterized and stored in inert atmosphere. Only few reports show a reproducible bi-stable behavior under ambient atmosphere. Among them, Jo et al. [28] developed a non-volatile memory element incorporating fullerene derivatives into the nanostructure of self-assembled poly(styrene-b-methyl methacrylate) (PS_{10}-b-$PMMA_{130}$) di-block copolymer. They demonstrated that such devices can be cycled more than 40 times and are characterized by a retention time of almost 1 h. Kim et al. [29] observed better results using a polyfluorene derivative film with silver nanoparticles, achieving retention time of 10^4 s with a reproducible behavior over more than 10^4 cycles. Very high retention times were also reported by Son et al. [30] using graphene sandwiched between two insulating poly(methyl methacrylate) (PMMA) layers. They demonstrated that these devices can be measured in ambient atmosphere with a number of ON/OFF switching cycles of around 1.5×10^5 and a (measured) retention time larger than 1×10^5 s. Hwang et al. [31] obtained highly environmental stable non-volatile memory elements with endurance cycle bigger than 10^2 and retention time in the order of 10^5 s, employing doped carbon nanotubes embedded into a polystyrene matrix. Summarizing, the demonstration of

significant improvements in organic RRAMs in terms of retention time under ambient atmosphere should represent the main aim and motivation for further research in this area.

In this paper, a novel non-volatile memory device based on the combination of an air-stable organic semiconductor and inorganic nanoparticles is proposed. The device is particularly conceived for allowing long-term data storage in ambient conditions with high ON/OFF ratios. A complete electrical characterization of the memory element will be provided, together with an in-depth morphological investigation of the structure in order to precisely define its working principle.

2. Experimental section

2.1. Structure and materials

The memory devices fabricated in this study are two terminal elements, consisting of an hybrid layer between a cross-point array of top and bottom electrodes. The hybrid layer is a nanocomposite material obtained by sandwiching a metal nanoparticles interlayer between two organic semiconductor layers. The schematic view of the device structure is shown in Fig. 1. In particular, a commercially available perylene derivative, namely N1400 (Polyera), was used as semiconductor layer of the resistive memories. It is an n-type semiconductor, which can be deposited by thermal evaporation but also from liquid phase since it is soluble in chlorinated solvents. Moreover, it shows stable performances in ambient conditions. Indium Tin Oxide (ITO) and silver (Ag) were used as bottom and top electrodes, respectively. Two different types of metal nanoparticles, namely aluminum (AlNPs) and gold (AuNPs), were employed for the intermediate layer.

2.2. Chemicals

Gold nanoparticles were synthesized according to chemical reduction method previously described in [32]. Briefly, a mixture of sodium citrate tribasic dihydrate (0.9 g, 1 wt%, Sigma Aldrich ⩾99.0%) and tannic acid (0.8 g, 1 wt%, Fluka) was added to the boiling aqueous chloroauric acid solution (98 g, 0.009 wt%, Sigma–Aldrich, ⩾49%) under reflux. The color of the solution immediately changed from yellow to dark red, as a result of the gold NPs formation. Afterwards, the mixture was stirred for additional 15 min and then cooled down to room temperature. The NPs final concentration was 50 ppm with an average size of 9 ± 2 nm.

2.3. Device fabrication

ITO/N1400/NPs/N1400/Ag memories were fabricated on Indium Thin Oxide (ITO) coated glass (KINTEC) substrates (2.5×2.5 cm^2). The ITO bottom electrodes were patterned directly on the ITO coated glass substrates by means of photolithography. Chemical etching on ITO was performed using zinc powder and hydrochloridric acid. The first N1400 layer was thermally evaporated with a
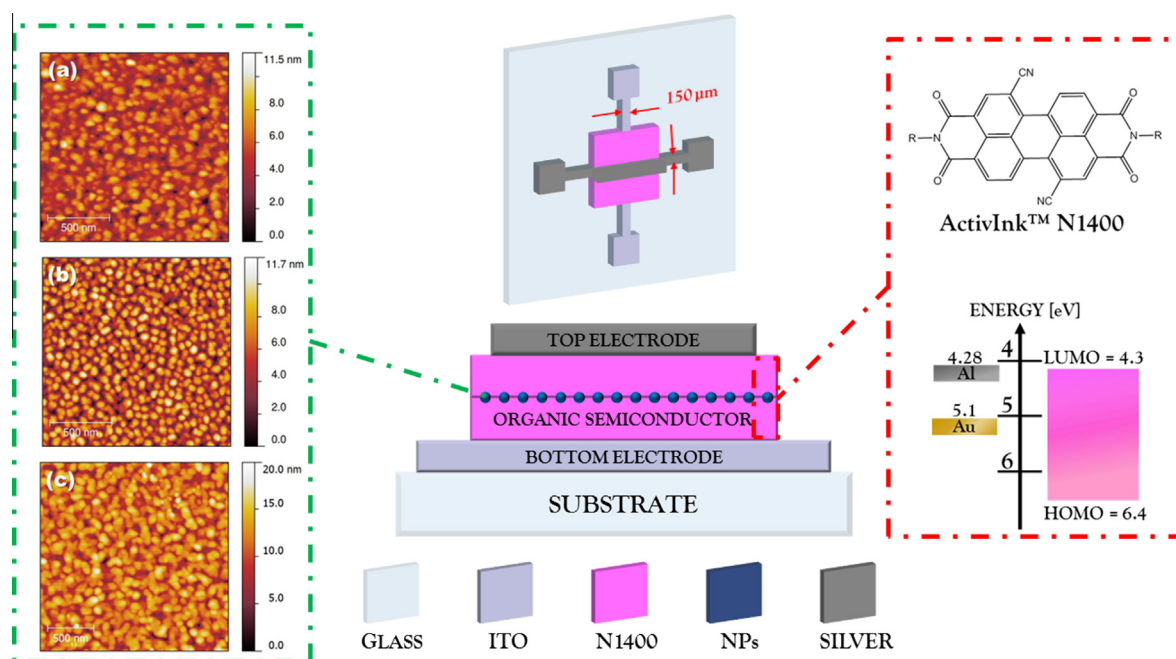
Fig. 1. Schematic view of the layered memory element. The right inset shows the chemical structure of N1400 and a schematic energy-level diagram of the ITO/N1400/metal nanoparticles/N1400/Ag device. The left inset shows AFM images: (a) N1400 surface (RMSR = 1.4 ± 0.2 nm); (b) evaporated AlNPs on N1400 surface (RMSR = 1.9 ± 0.2 nm) and (c) electrosprayed AuNPs on N1400 surface (RMSR = 2.3 ± 0.2 nm).

deposition rate of 1 Å/s. Aluminum NPs were deposited by thermal evaporation with a deposition rate of 0.5 Å/s. The nominal thickness of such interlayer is 15 nm. It has been shown that in similar conditions the aluminum layer does not form a continuous film [19,25,26]. Gold nanoparticles were deposited by means of electrospraying: 6 ml of purified colloid were obtained by several cycles of centrifugations and adding deionized water. The solution actually employed in the electrospraying equipment was obtained by mixing 2 ml of purified colloid, 1 ml of deionized water and 1 ml of pure ethyl alcohol (96%). A single jet deposition mode was employed, with applied voltage ranging from 6 to 7 kV and with a distance between the nozzle and the substrate of 2 cm. The second semiconductor layer was deposited in the same way as the first one and the nominal thickness of the total organic bi-layer is 240 nm. Both N1400 and aluminum nanoparticles were thermally evaporated at a pressure of about 10^{-5} Torr monitoring the film thickness with a quartz crystal microbalance. Finally, the devices were completed by thermal evaporation of the top silver electrodes using a shadow mask.

2.4. Electrical and morphological characterization

Electrical measurements were performed in ambient conditions (temperature of about 22 °C, humidity in the order of 50%, ambient light) with an HP – Agilent 4155A Semiconductor Parameter Analyzer or a Keithley 2636.

The morphology of the thin films was characterized using atomic force microscopy (AFM) in intermittent contact mode (JPKNanoWizard II). Gwyddion software was used for the post-processing and analysis of the AFM data.

A structural characterization was performed with High resolution X-ray Photoelectron Spectroscopy (HR-XPS) and Time of Flight Secondary Ion Mass Spectrometry (ToF-SIMS). In particular, XPS depth profile was obtained by alternating sputtering with monoatomic argon beam (1 keV) followed by the XPS analysis (ESCALAB spectrometer, Thermo Scientific). ToF-SIMS analysis was performed with a dual beam system (ToF-IV, by ION-TOF) equipped with a $Bi^{(3+)}$ cluster gun for the analysis, and a 500 eV $Cs^{(+)}$ gun for the material sputtering. In both cases, the sputtering time was converted to a depth by measuring the crater depth after the depth profile.

3. Results and discussion

3.1. Electrical characterization

At first, the resistive switching behavior was evaluated by acquiring the $I–V$ characteristics of the devices; an example of them is reported in Fig. 2(a), where the left y-axis is referred to the AlNPs based memories and the right one is referred to the AuNPs based memories. The devices showed a clear resistive switching behavior and similar operational characteristics with both types of NPs. The typical switching effect is obtained by sweeping the bias voltage from negative to positive values, and back. This allows determining the writing and erasing voltages, i.e. the threshold voltages that cause the device switching from its high resistance state (HRS, OFF-state) to its low resistance state (LRS, ON-state) and back, respectively. The initial state of the memory device can be a LRS state or a HRS. When the initial state is a LRS and the applied bias exceeds
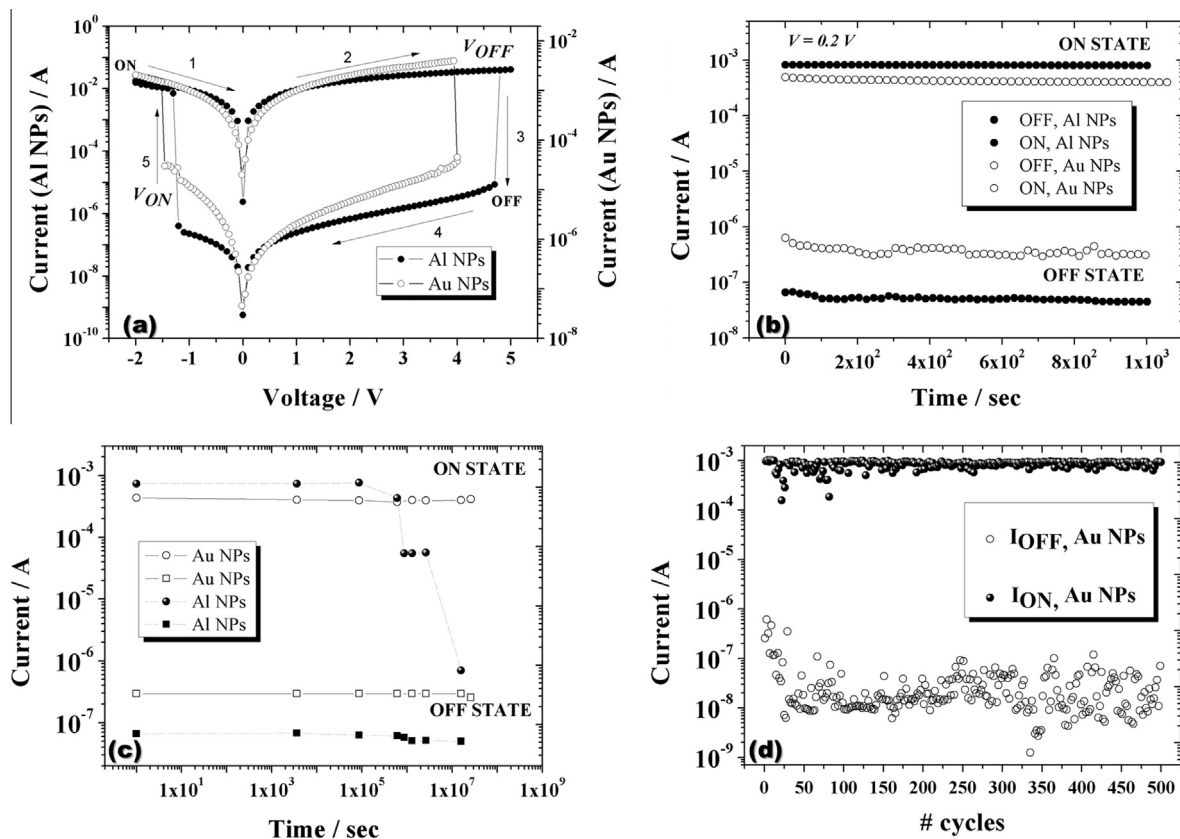
Fig. 2. Comparison between memory elements employing Al and Au as metal interlayer: (a) Typical *I–V* curves (the left *y*-axis is referred to the AlNPs based memories and the right one is referred to the AuNPs based memories); (b) endurance tests; (c) retention time tests and (d) cycling test performed after 16 months on AuNPs based devices.

a threshold value V_{OFF} (whose average value is $(+3.1 \pm 0.6)$ V for AuNPs, and (5.0 ± 1.0) V for AlNPs), the resistance of the device increases abruptly by several orders of magnitude. During the reverse voltage sweep, an abrupt current increase occurs at a critical voltage V_{ON} (whose average value is (-1.6 ± 0.4) V for AuNPs, and (-1.4 ± 0.4) V for AlNPs) and the device switches from the HRS back to the LRS. The voltage range between V_{ON} and V_{OFF} is the region of bi-stability: the state of the device can be read by applying a voltage within this range, but significantly far from its limits. The ON state can be set by applying a voltage pulse $V_{SET} < V_{ON}$ and the OFF state can be reset by applying a voltage $V_{RESET} > V_{OFF}$. The ratio between the currents recorded in the 2 states (I_{ON}/I_{OFF}), at the same reading voltage $V_{READ} = 0.2$ V, is typically 10^4 for AlNPs and 10^3 for AuNPs (Fig. 2(b)). Thanks to this large separation between the two resistance states, large noise margins can be obtained, so that the ON and OFF states are clearly distinguishable for readout electronics. More details on the statistics of the tested devices are reported in Fig. S4 of the Supporting Information.

In order to complete the investigation of the memory performance, endurance and retention time tests were carried out. Fig. 2(b) shows representative data from the endurance tests. Voltage stress tests were performed by applying to the device a continuous readout voltage of

0.2 V for about 10^3 s in both ON and OFF states. It is noteworthy that a steady current level is perfectly maintained in both states, thus proving that the device is stable and not affected by bias stress even for a continuous reading time well beyond the one employed in routine applications.

The widespread diffusion of organic memories is essentially limited by their retention capability. For this reason, the retention time for both ON and OFF states was investigated periodically at a reading voltage of 0.2 V. As shown in Fig. 2(c), a retention time of $\sim 1.5 \times 10^7$ s (~ 6 months) was obtained for devices with AuNPs. In addition, at this time, the originally programmed devices were erased and re-written resulting in OFF and ON states that are exactly the same as the initial ones (Fig. S1(a)). Furthermore, reading performed after another ten months (thus on devices belonging to a batch fabricated 16 months before the last retention test) allowed recording a new value of retention time of $\sim 2.6 \times 10^7$ s and showed that these devices have a lifetime of at least 16 months. Fig. 2(c) clearly demonstrates the stability of the ON/OFF ratio during this period of time. Endurance tests were also performed (Fig. S1(c)) at different times (0, 6 and 12 months), demonstrating the reliability of the stored data also after several months from the original measurements. It is noteworthy that the

devices were measured and stored in ambient conditions for the whole period of investigation, thus lending weight to the stability of the memory in air. For the devices made with AlNPs, a lower retention time was observed, as shown in Fig. 2(c). Moreover, as shown in Fig. S1(b), the original ON and OFF states were not recovered in tests carried out after several months. The actual reasons behind the degradation of the device performances with AlNPs are still under investigation. However, it is possible to hypothesize that the oxidation of AlNPs, induced by the oxygen diffusion within the organic matrix, may play a role, but this needs to be further investigated. In order to test the operational lifetime, writing/erasing cycles were performed on AuNPs based devices after 16 months from the fabrication. Fig. 2(d) shows and demonstrates that such devices are able to reach, at this time, at least 500 cycles.

### 3.2. Morphological and structural characterization

The morphology of N1400 and of the NPs layer over the N1400 surface was investigated by means of Atomic Force Microscopy (AFM). For the bare N1400 surface, (Fig. 1(a)) a root mean square surface roughness (RMSR) of about 1.4 ± 0.2 nm was found. Fig. 1(b) and (c) shows AlNPs (RMSR = 1.9 ± 0.2 nm) and AuNPs (RMSR = 2.3 ± 0.2 nm) on N1400 surfaces, respectively. It is clearly evident that the surface roughness of the N1400 is not substantially varied after the deposition of both kinds of metal NPs. This leads to the conclusion that the morphology of the nano-composite hybrid film is dominated by the one of the underlying organic semiconductor. Moreover, it is possible to observe that AuNPs and AlNPs on N1400 surface seem to be very similar in size, even if they were deposited with different techniques and the AuNPs had a very small average size of 9 ± 2 nm in colloid (before deposition by electrospraying). This confirms that the final morphology of the nanoparticles film is likely driven by the characteristics of the N1400 film.

In order to shed light on the switching behavior of the proposed devices, a structural characterization was performed with High resolution X-ray Photoelectron Spectroscopy (HR-XPS) and Time of Flight Secondary Ion Mass Spectrometry (ToF-SIMS). Such techniques allow evaluating the material composition of multilayered devices. In this work, they were employed for investigating the possible formation of metallic filaments, which has been recently suggested being the driving mechanism for resistive switching in many organic bi-stable devices [33]. In particular, XPS and ToF-SIMS depth profiles were carried out on pristine and conditioned (written/erased/re-written several times) memories to quantitatively and spatially characterize the possible metal penetration inside the organic layer. Metal diffusion could occur during the top electrode evaporation and/or could be assisted by electrical field diffusion during the memory testing. The presence of point-like structures at the top electrode/organic interface was proposed to be fundamental for metallic filament growth in organic memories [34].

Fig. 3(a) shows a typical XPS depth profile obtained on a pristine memory by alternating cycles of sputtering with argon ion beam and XPS analysis. The Ag$_{3d}$ peak area (in log scale) is shown as a function of the sputtering depth. Interestingly, silver is present through the entire N1400 depth, as the mean atomic percentage over the analysis area of 200×200 μm^2 is still 0.1% close to the bottom electrode (P4). The HR spectra obtained at the corresponding depths are indicated and compared in the inset. The size-dependent binding energy shift of the Ag$_{3d}$ peak (evidenced by the vertical bar in the inset) comes from electrostatic interaction between the leaving photoelectron and the positive charge left on the small supported cluster (typically <5 nm) surface during the photoemission process [35]. The NPs signal was too weak to be quantified with XPS.

Dual beam ToF-SIMS imaging was performed to increase the sensitivity, and study the spatial distribution of elements with 1×1 μm^2 (in-plane) $\times 1$ nm in depth resolution. Fig. 3(b) and (c) shows respectively the ToF-SIMS depth profiles obtained on a pristine (b) and on a cycled (c) device finally set into the ON state. A higher silver diffusion is evident in the electrically stressed device. The spatial distribution of silver, indium and gold (in red, green and blue color scale respectively) was studied on 120×120 μm^2 maps, showing a clear inhomogeneous Ag diffusion in channel-like structures (filaments) which protracts through the entire N1400 layer till the ITO bottom electrode in electrically stressed devices (see Fig. 3(e)). The sparse distribution of such filamentary paths suggests that the formation could be driven by defects in the organic layer. Pristine devices (Fig. 3(d)) showed a weaker silver diffusion extending at most 50 nm under the Ag/N1400 interface, i.e. never determining a continuous electrical path between the electrodes. Field assisted diffusion of silver atoms during I–V scans appears necessary to establish a complete "filament" bridging the two metal electrodes. The presence of few diffusion areas and the fact that no differences were evidenced by the comparison of devices set into the LRS or into the HRS suggest that the same diffusion path could be locally activated and deactivated (ruptured) during the memory cycling, allowing a reproducible switching, as observed in the I–V testing. Weak signals from the metal interlayer were evidenced by ToF-SIMS analysis. Resistive switching in devices without metal NPs resulted considerably less reproducible and reliable (see Supporting Information, Fig. S3); this suggests that the NPs play an essential role in assisting the filament growth and in stabilizing its dynamics during conditioning. Indeed, considering the ToF-SIMS images in Fig. 3 (and in Fig. S2), where pristine (Fig. 3d) and conditioned (Fig. 3e) devices are compared, a very different nanoparticles distribution can be noticed. In particular, NPs are almost uniformly distributed in pristine devices (Fig. 3d and Fig. S2c). On the contrary, in conditioned devices, it is possible to observe a coalescence of AuNPs in correspondence of Ag filaments (Fig. 3e and Fig. S2f). This behavior suggests that NPs could actually diffuse within the organic matrix, acting as seeds for filaments formation and growth. This feature seems to play a crucial role in improving the stability and reproducibility of the switching behavior, just as already observed for inorganic resistive-switching devices [36,37].
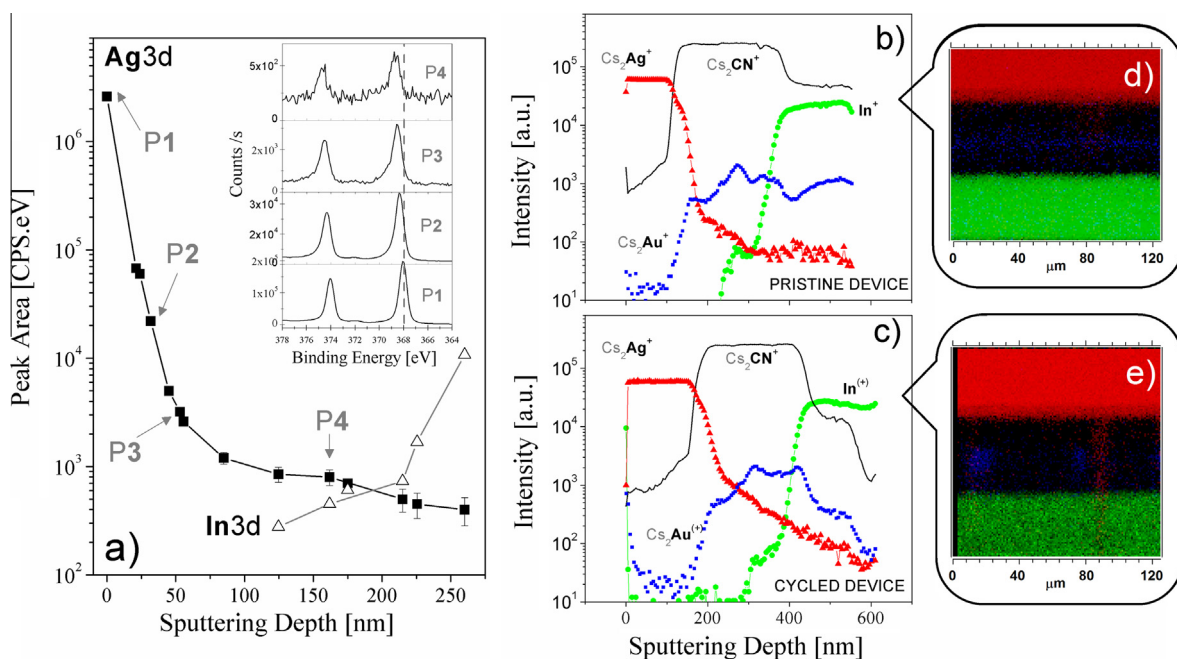
Fig. 3. (a) XPS depth profile of a pristine Ag/(N1400 + AuNPs)/ITO memory element showing the Ag_{3d} and In_{3d} peak area as a function of the sputtering depth. The inset shows the vertically stacked HR Ag_{3d} spectra obtained at the corresponding points (depths) indicated in panel (a): the spectra have been displayed with the appropriate y-scale to help the comparison. The dashed vertical line is to guide the visualization of the binding energy shifts. (b)–(c) ToF-SIMS depth profiles obtained on a pristine (b) and operated (c) device showing the intensity of the signal of silver (Cs_2Ag^+, red triangles), indium (In^+, green dots), a N1400 fragment (Cs_2CN^+, grey line) and gold (Cs_2Au^+, blue dots) as a function of the sputtering depth. An enhanced Ag diffusion is evident in the operated device. (d)–(e) Two dimensional (XZ) cross sections extrapolated from the 3D ToF-SIMS images corresponding to (b) and (c) profiles (same color label) showing an Ag filament in the operated device. (For interpretation of the references to color in this figure legend, the reader is referred to the web version of this article.)

4. Conclusions

In conclusion, a novel non-volatile hybrid organic–inorganic memory structure, which is air-stable for over 16 months, has been presented. A commercially available, environmentally stable, n-type organic semiconductor was employed as organic matrix. This work clearly demonstrates the suitability of such a material in the fabrication of memory elements, employing different metal NPs as intermediate layer. However, with AuNPs, a retention time of at least ten months was reproducibly demonstrated for devices stored in ambient conditions for sixteen months in total; in addition, after this time, the functionality of the devices in terms of writing, reading and erasing was perfectly maintained. With AlNPs, the device is less stable, showing not only a shorter retention time, but also the degradation of the ON and OFF states after less than 6 months from the fabrication. These results suggest that environmental stability of both organic and inorganic materials is needed for obtaining reproducible and stable memory effects. The proposed structure was thoroughly characterized by surface sensitive (AFM) and depth profile (XPS and ToF-SIMS) techniques. The results clearly evidence the top electrode material diffusion inside the organic layer. Resistive switching mechanisms in this material can thus be interpreted in terms of formation and rupture of metallic filaments inside the organic layer assisted by the metal NPs. Further investigations are in

progress in order to achieve a full comprehension of the degradation mechanisms for AlNPs, to better control the filament dynamics and to increase the device reliability.

Appendix A. Supplementary material

Supplementary data associated with this article can be found, in the online version, at http://dx.doi.org/10.1016/j.orgel.2015.01.001.

References

[1] Y. Vaynzof, D. Kabra, T.J.K. Brenner, H. Sirringhaus, R.H. Friend, Recent advances in hybrid optoelectronics, Isr. J. Chem. 52 (2012) 496.
[2] S. Gunes, H. Neugebauer, N.S. Sariciftci, Conjugated polymer-based organic solar cells, Chem. Rev. 107 (2007) 1324–1338.
[3] L. Kergoat, B. Piro, M. Berggren, G. Horowitz, M.-C. Phan, Advances in organic transistor-based biosensors: from organic electrochemical transistors to electrolyte-gated organic field-effect transistors, Anal. Bioanal. Chem. 402 (2012) 1813–1826.

[4] P. Lin, F. Yan, Organic thin-film transistors for chemical and biological sensing, Adv. Mater. 24 (2012) 34–51.

[5] S.R. Forrest, The path to ubiquitous and low-cost organic electronic appliances on plastic, Nature 428 (2004) 911–918.

[6] H. Klauk, U. Zschieschang, J. Pflaum, M. Halik, Ultralow-power organic complementary circuits, Nature 445 (2007) 745–748.

[7] T. Sekitani, Y. Noguchi, U. Zschieschang, H. Klauk, T. Someya, Organic transistors manufactured using inkjet technology with subfemtoliter accuracy, Proc. Natl. Acad. Sci. U.S.A. 105 (2008) 4976–4980.

[8] S.I. Na, S.-S. Kim, J. Jo, D.-Y. Kim, Efficient and flexible ITO-free organic solar cells using highly conductive polymer anodes, Adv. Mater. 20 (2008) 4061–4067.

[9] T. Sekitani, H. Nakajima, H. Maeda, T. Fukusima, T. Aida, K. Hata, T. Someya, Stretchable active-matrix organic light-emitting diode display using printable elastic conductors, Nat. Mater. 8 (2009) 494–499.

[10] H. Yan, Z. Chen, Y. Zheng, C. Newman, J.R. Quinn, F. Dotz, M. Kastler, A. Facchetti, A high-mobility electron-transporting polymer for printed transistors, Nature 457 (2009) 679–686.

[11] D. Prime, S. Paul, Overview of organic memory devices, Philos. Trans. R. Soc. A 367 (2009) 4141–4157.

[12] R.C.G. Naber, K. Asadi, P.W.M. Blom, D.M. de Leeuw, B. de Boer, Organic nonvolatile memory devices based on ferroelectricity, Adv. Mater. 22 (2010) 933–945.

[13] T. Sekitani, T. Yokota, U. Zschieschang, H. Klauk, S. Bauer, K. Takeuchi, M. Takamiya, T. Sakurai, T. Someya, Organic nonvolatile memory transistors for flexible sensor arrays, Science 326 (2009) 1516–1519.

[14] R. Waser, M. Aono, Nanoionics-based resistive switching memories, Nat. Mater. 6 (2007) 833–840.

[15] J.C. Scott, L.D. Bozano, Nonvolatile memory elements based on organic materials, Adv. Mater. 19 (2007) 1452–1463.

[16] B. Cho, S. Song, Y. Ji, T.-W. Kim, T. Lee, Organic resistive memory devices: performance enhancement, integration, and advanced architectures, Adv. Funct. Mater. 21 (2011) 2806–2829.

[17] T. Lee, Y. Chen, Resistive switching phenomena in thin films: materials, devices, and applications, MRS Bull. 27 (2012) 144–149.

[18] L.P. Ma, J. Liu, Y. Yang, Organic electrical bistable devices and rewritable memory cells, Appl. Phys. Lett. 80 (2002) 2997–2999.

[19] L.P. Ma, S.M. Pyo, J.Y. Ouyang, Q.F. Xu, Y. Yang, Nonvolatile electrical bistability of organic/metal-nanocluster/organic system, Appl. Phys. Lett. 82 (2003) 1419–1421.

[20] J. Ouyang, C.-W. Chu, C.R. Szmanda, L. Ma, Y. Yang, Programmable polymer thin film and non-volatile memory device, Nat. Mater. 3 (2004) 918–922.

[21] C.-W. Chu, J. Ouyang, J.H. Tseng, Y. Yang, Organic donor–acceptor system exhibiting electrical bistability for use in memory devices, Adv. Mater. 17 (2005) 1440–1443.

[22] R.J. Tseng, J. Huang, J. Ouyang, R.B. Kaner, Y. Yang, Polyaniline nanofiber/gold nanoparticle nonvolatile memory, Nano Lett. 5 (2005) 1077–1080.

[23] Y. Yang, J.Y. Ouyang, L.P. Ma, R.J.-H. Tseng, C.-W. Chu, Electrical switching and bistability in organic/polymeric thin films and memory devices, Adv. Funct. Mater. 16 (2006) 1001–1014.

[24] L.D. Bozano, B.W. Kean, V.R. Deline, J.R. Salem, J.C. Scott, Mechanism for bistability in organic memory elements, Appl. Phys. Lett. 84 (2004) 607–609.

[25] L.D. Bozano, B.W. Kean, M. Beinhoff, K.R. Carter, P.M. Rice, J.C. Scott, Organic materials and thin-film structures for cross-point memory cells based on trapping in metallic nanoparticles, Adv. Funct. Mater. 15 (2005) 1933–1939.

[26] V.S. Reddy, S. Karak, S.K. Ray, A. Dhar, Carrier transport mechanism in aluminum nanoparticle embedded AlQ$_3$ structures for organic bistable memory devices, Org. Electron. 10 (2009) 138–144.

[27] X. Liu, Z. Ji, L. Shang, H. Wang, Y. Chen, M. Han, C. Lu, M. Liu, J. Chen, Organic programmable resistance memory devices based on Au/AlQ$_3$/gold-nanoparticles/AlQ$_3$/Al structure, IEEE Electron. Dev. Lett. 32 (2011) 1140–1142.

[28] H. Jo, J. Ko, J.A. Lim, H.J. Chang, Y.S. Kim, Organic nonvolatile resistive switching memory based on molecularly entrapped fullerene derivative within a diblock copolymer nanostructure, Macromol. Rapid Commun. 34 (2013) 355–361.

[29] T.-W. Kim, S.-H. Oh, H. Choi, G. Wang, D.-Y. Kim, H. Hwang, T. Lee, Effect of Ag nanoparticles on resistive switching of polyfluorene-based organic non-volatile memory devices, J. Korean Phys. Soc. 56 (2010) 128–132.

[30] D.I. Son, T.W. Kim, J.H. Shim, J.H. Jung, D.U. Lee, J.M. Lee, W. Il Park, W.K. Choi, Flexible organic bistable devices based on graphene embedded in an insulating poly(methyl mathacrylate) polymer layer, Nano Lett. 10 (2010) 2441–2447.

[31] S.K. Hwang, J.M. Lee, S. Kim, J.S. Park, H. Il Park, C.W. Ahn, K.J. Lee, T. Lee, S.O. Kim, Flexible resistive memory with controlled charge trap B- and N-doped carbon nanotubes, Nano Lett. 12 (2012) 2217–2221.

[32] K. Soliwoda, E. Tomaszewska, B. Tkacz-Szczesna, E. Mackiewicz, M. Rosowski, A. Bald, C. Blanck, M. Schmutz, J. Novak, F. Schreiber, G. Celichowski, J. Grobelny, Effect of the alkyl chain length of secondary amines on the phase transfer of gold nanoparticles from water to toluene, Langmuir 30 (2014) 6684–6693.

[33] S. Nau, S. Sax, E.J.W. List-Kratochvill, Unravelling the nature of unipolar resistance switching in organic devices by utilizing the photovoltaic effect, Adv. Mater. 26 (2014) 2508–2513.

[34] Y.T. You, Q. Zeng, Y. Yao, M.L. Wang, B. Wu, Y. He, Y.M. Hu, C.Q. Wu, X.Y. Hou, Field-induced evolution of metallic nano-tips in indium tin oxide-tris-(8-hydroxyquinoline) aluminum–aluminum device, Appl. Phys. Lett. 100 (2012) 123304.

[35] Y. Busby, J.J. Pireaux, Metal nanoparticle size distribution in hybrid organic/inorganic films determined by high resolution X-ray photoelectron spectroscopy, J. Electron. Spectrosc. Relat. Phenomena 192 (2014) 13–18.

[36] Q. Liu, S. Long, W. Wang, S. Tanachutiwat, Y. Li, Q. Wang, M. Zhang, Z. Huo, J. Che, M. Liu, Low-power and highly uniform switching in ZrO$_2$-based ReRAM with a Cu nanocrystal insertion layer, Electron. Dev. Lett., IEEE 31 (2010) 1299–1301.

[37] Q. Liu, S. Long, H. Lv, W. Wang, J. Niu, Z. Huo, J. Chen, M. Liu, Controllable growth of nanoscale conductive filaments in solid-electrolyte-based ReRAM by using a metal nanocrystal covered bottom electrode, ACS Nano 4 (2010) 6162–6168.